Cold isospin asymmetric baryonic rich matter in nonlocal NJL-like models

J. P. Carlomagno,[1,*] D. Gómez Dumm,[1] and N. N. Scoccola[2,3]

[1]*IFLP, CONICET—Departamento de Física, Facultad de Ciencias Exactas, Universidad Nacional de La Plata, C.C. 67, 1900 La Plata, Argentina*

[2]*CONICET, Rivadavia 1917, 1033 Buenos Aires, Argentina*

[3]*Physics Department, Comisión Nacional de Energía Atómica, Avenida del Libertador 8250, 1429 Buenos Aires, Argentina*

(Received 26 February 2024; revised 25 April 2024; accepted 3 May 2024; published 28 May 2024)

We study the features of low energy strong interactions for a system at zero temperature and finite baryon and isospin chemical potentials, in the framework of a Nambu–Jona-Lasinio-like model that includes nonlocal four-point interactions. We analyze the phase transitions corresponding to chiral symmetry restoration and pion condensation, comparing our results with those obtained from local NJL-like models and lattice QCD calculations.

DOI: 10.1103/PhysRevD.109.094041

I. INTRODUCTION

Over the past few decades, there has been a significant amount of research focused on the study of quark and hadronic matter under conditions of finite temperature T and baryon chemical potential μ_B. At high temperatures and low densities, it is well known that quantum chromodynamics (QCD) predicts the formation of a quark-gluon plasma (QGP) [1], in which quarks and gluons are expected to be weakly coupled. In this limit, strong interactions can be described through perturbative calculations based on expansions in powers of the QCD coupling constant. In the region of intermediate temperatures one can rely on lattice QCD (LQCD) calculations, which indicate that at vanishing chemical potential the transition from the hadronic phase to the QGP occurs in the form of a smooth crossover [2]. On the other corner of the $\mu_B - T$ phase diagram, at sufficiently high densities and low temperatures, one expects to find a "color-flavor locked" phase, in which the existence of strongly correlated quark pairs is predicted [3]. At moderate densities, however, the situation is much more uncertain. The main reason for this is that first-principle nonperturbative QCD calculations at nonzero μ_B are hardly accessible by Monte Carlo simulations, due to the presence of a complex fermion determinant in the corresponding partition function (the so-called "sign problem") [4]. In this region most theoretical analyses of the phase structure rely on the predictions from effective models for strong interactions.

In addition to T and μ_B, the system may show an imbalance in the isospin charge, which can be characterized by an isospin chemical potential μ_I. This situation, which can be applicable, e.g., to the study of the physics of heavy ion collisions and the structure of stellar objects, is worth considering in order to get more insight into the properties of strongly interacting matter. In general, the QCD phase diagram in the T-μ_B-μ_I thermodynamic space is expected to show a rich structure that can be addressed both from LQCD techniques and effective approaches to strong interactions [5–25]. In the case of systems at $\mu_B = 0$ and finite μ_I, LQCD calculations are not affected by the sign problem [26]; thus, the corresponding phase diagram in the $T - \mu_I$ plane has been studied in several works that use different lattice techniques [21,27–31]. In particular, one important feature confirmed by these calculations is that at $\mu_I \simeq m_\pi$ one finds the onset of a Bose-Einstein pion condensation phase [5,32], which could enable the existence of pion stars [33].

In the case of nonzero μ_B and μ_I, LQCD analyses are not free from the sign problem and require some extrapolations. Hence, it is remarkably important to get definite predictions from effective models. In this work we study the properties of quark matter under finite μ_B and μ_I conditions considering quark models in which the fermions interact through covariant *nonlocal* four-point couplings [34]. These models can be viewed as improved versions of the standard (local) Nambu–Jona-Lasinio (NJL) scheme [35,36]. In fact, the nonlocal character of the interactions arises naturally in the context of several successful approaches to low-energy quark dynamics, such as the instanton liquid model [37] and the Schwinger-Dyson resummation techniques [38,39]. It is also seen that this approach leads to a momentum

*carlomagno@fisica.unlp.edu.ar

dependence in the quark propagator that can be consistently matched [40] to LQCD results [41,42]. Moreover, it has been found that it is possible to derive the main features of this type of model starting directly from QCD [43]. The so-called "nonlocal NJL" (nlNJL) models have the virtue of avoiding some of the drawbacks observed in the local approach. For example, through the usage of well-behaved nonlocal form factors, it is possible to regularize ultraviolet loop integrals while preserving anomalies [44] and ensuring proper charge quantization. In addition, the absence of sharp cutoffs implies that model predictions are more stable against changes in the input parameters [45].

Within this framework, in a previous work [46] we have studied the phase diagram in the $\mu_I - T$ plane for $\mu_B = 0$, finding a good agreement with LQCD calculations. In the present article our aim is to complement this previous research, considering now a system at finite μ_I and μ_B. We study in detail the condensate formation and the corresponding phase transitions, and compare our findings with those obtained from the local NJL model [47–50]. For the moment we restrict ourselves to zero temperature. It is worth mentioning that a further extension to finite temperature systems should require the incorporation of thermodynamic aspects of confinement, which are usually implemented by including the interaction between the quarks and the Polyakov loop [51,52]. The local NJL is extended in this way to a Polyakov–Nambu–Jona-Lasinio (PNJL) model [53–59], where chiral restoration and deconfinement transitions can be addressed through a common framework. A similar extension can be carried out in the case of the nonlocal approach, assuming that the quarks interact with a background color field (see, e.g., Refs. [60–65]). It has to be remarked that the new interactions also involve an effective Polyakov-loop potential, which introduces some additional uncertainty in the theoretical predictions. To complete the general picture, we also mention that effective NJL-type models predict the presence of several distinct regions in the phase diagram [66]. For instance, one may encounter inhomogeneous phases characterized by vacuum expectation values that break translational invariance [67–70]. Additionally, one can find regions populated by "quarkyonic" matter, in which chiral symmetry is approximately restored while quarks still remain subject to confining interactions [71–73].

Within the above described nlNJL model, we also analyze here the behavior of the speed of sound c_s in the presence of nonzero isospin chemical potential. Recent LQCD calculations [31] have found that c_s^2 reaches a maximum at intermediate values of μ_I ($\mu_I \sim 2m_\pi$) and then decreases slowly towards the limit predicted by duality for 4D conformal field theories [74]. This result has been discussed in the framework of several effective models; see Refs. [75–79]. We also consider the relation between the speed of sound and the trace anomaly [80], which measures the amount of violation of conformal symmetry. A previous analysis of the behavior of the trace anomaly in this context has been presented in Ref. [46].

This article is organized as follows. In Sec. II we present the general formalism to describe two-flavor nlNJL models at zero temperature and finite baryon and isospin chemical potential, including theoretical expressions for chiral and pion condensates and for the speed of sound. In Sec. III we discuss our numerical results for condensates and phase transitions, for both vanishing and nonvanishing μ_B. Finally, in Sec. IV we summarize our results and present our main conclusions.

II. THEORETICAL FORMALISM

We consider a two-flavor quark model that includes nonlocal scalar and pseudoscalar quark-antiquark currents. The Euclidean action reads [46]

$$S_E = \int d^4x \left[\bar{\psi}(x)(-i\not{\partial} + \hat{m})\psi(x) - \frac{G}{2} j_a(x) j_a(x)\right], \quad (1)$$

where $\psi = (\psi_u \psi_d)^T$ stands for the u, d quark field doublet, and $\hat{m} = \mathrm{diag}(m_u, m_d)$ is the current quark mass matrix. For simplicity, we assume that the current quark masses m_u and m_d are equal, and we denote them generically by m_c. The nonlocal currents $j_a(x)$ in Eq. (1) are given by

$$j_a(x) = \int d^4z\, \mathcal{G}(z)\, \bar{\psi}\left(x + \frac{z}{2}\right) \Gamma_a \psi\left(x - \frac{z}{2}\right), \quad (2)$$

where we have defined $\Gamma_a = (\mathbb{1}, i\gamma_5 \vec{\tau})$, with τ_i being Pauli matrices that act on flavor space. The function $\mathcal{G}(z)$ is a form factor responsible for the nonlocal character of the four-point interactions. The action for the standard (local) two-flavor quark version of the NJL model is recovered by taking $\mathcal{G}(z) = \delta^{(4)}(z)$.

To study strongly interacting matter in a system at nonzero chemical potential, we introduce the partition function $\mathcal{Z} = \int \mathcal{D}\bar{\psi}\mathcal{D}\psi \exp[-S_E]$. As stated, we are interested in studying isospin asymmetric matter; this can be effectively implemented by introducing quark chemical potentials μ_u and μ_d that, in general, are different from each other. Thus, we consider the effective action in Eq. (1) and perform the replacement

$$\begin{pmatrix} \partial_4 & 0 \\ 0 & \partial_4 \end{pmatrix} \to \begin{pmatrix} \partial_4 - \mu_u & 0 \\ 0 & \partial_4 - \mu_d \end{pmatrix}. \quad (3)$$

In fact, it is convenient to write the quark chemical potentials in terms of average and isospin chemical potentials denoted by μ ($= \mu_B/3$) and μ_I, respectively. One has

$$\mu_u = \mu + \frac{\mu_I}{2}, \qquad \mu_d = \mu - \frac{\mu_I}{2}. \quad (4)$$

In addition, owing to the nonlocal character of the interactions, to obtain the appropriate conserved currents, one has to complement the replacement in Eq. (3) with a modification of the nonlocal currents in Eq. (2). This procedure is similar to the one used, e.g., in Refs. [46,81,82].

We proceed now by carrying out a standard bosonization of the effective theory, introducing bosonic degrees of freedom σ and π_i, $i = 1, 2, 3$, and integrating out the fermionic fields. Then we consider a mean field approximation (MFA) in which the bosonic fields are replaced by their vacuum expectation values (VEVs) $\bar{\sigma}$ and $\bar{\pi}_i$. As is well known, in the chiral limit ($m_c = 0$), for $\mu_I = 0$ the action is invariant under global $\mathrm{U}(1)_B \otimes \mathrm{SU}(2)_I \otimes \mathrm{SU}(2)_{IA}$ transformations. The group $\mathrm{U}(1)_B$ is associated with baryon number conservation, while the chiral group $\mathrm{SU}(2)_I \otimes \mathrm{SU}(2)_{IA}$ corresponds to the symmetries under isospin and axial-isospin transformations. Now, in the presence of a nonzero isospin chemical potential, the full symmetry group is explicitly broken down to the $\mathrm{U}(1)_{I_3} \otimes \mathrm{U}(1)_{I_3 A}$ subgroup. If σ develops a nonzero VEV, the $\mathrm{U}(1)_{I_3 A}$ symmetry gets spontaneously broken. Moreover, while even for finite current quark masses one has $\bar{\pi}_3 = 0$ [83], for $\mu_I \neq 0$ it can happen that π_1 and π_2 develop nonvanishing VEVs, leading to a spontaneous breakdown of the remaining $\mathrm{U}(1)_{I_3}$ symmetry. Since the action is still invariant under $\mathrm{U}(1)_{I_3}$ transformations, without loss of generality one can choose $\bar{\pi}_i = \delta_{i1}\bar{\pi}$.

We consider the above described general situation in which both $\bar{\sigma}$ and $\bar{\pi}$ can be nonvanishing. The mean field grand canonical thermodynamic potential is found to be given by

$$\Omega^{\mathrm{MFA}} = \frac{\bar{\sigma}^2 + \bar{\pi}^2}{2G} - \mathrm{Tr}\,\ln\begin{pmatrix} \not{p}_u + M(p_u) & i\gamma_5\rho(\bar{p}) \\ i\gamma_5\rho(\bar{p}) & \not{p}_d + M(p_d) \end{pmatrix}, \tag{5}$$

where

$$M(p) = m_c + g(p)\bar{\sigma}, \qquad \rho(p) = g(p)\bar{\pi}. \tag{6}$$

Here we have defined $p_f \equiv (\vec{p}, p_4 + i\mu_f)$, with $f = u, d$, and $\bar{p} = (p_u + p_d)/2$. The function $g(p)$ is the Fourier transform of the form factor $\mathcal{G}(z)$ in Eq. (2). It is worth noticing that the presence of the covariant form factor $g(p)$ introduces an additional dependence on the chemical potentials μ and μ_I, in comparison with the case of the local NJL model.

As usual in this type of model, it is seen that Ω^{MFA} turns out to be divergent and has to be regularized. Here, we adopt a prescription similar to the one considered, e.g., in Refs. [46,84], in which one subtracts the thermodynamic potential obtained for $\bar{\sigma} = \bar{\pi} = 0$ and adds it in a regularized form. In this way, the regularized expression $\Omega^{\mathrm{MFA,reg}}$ is given by

$$\Omega^{\mathrm{MFA,reg}} = \frac{\bar{\sigma}^2 + \bar{\pi}^2}{2G} - 2N_c \int \frac{d^4p}{(2\pi)^4} \ln\left[\frac{D(\bar{\sigma}, \bar{\pi})}{D(0,0)}\right] + \Omega^{\mathrm{free,reg}}, \tag{7}$$

where

$$D(\bar{\sigma}, \bar{\pi}) = E_u^2 E_d^2 - \rho(\bar{p})^2[(M(p_u) - M(p_d))^2 - (\mu_u - \mu_d)^2], \tag{8}$$

with $E_f^2 = M(p_f)^2 + p_f^2 + \rho(\bar{p})^2$. The regularized form of the free piece, after subtraction of divergent terms, reads

$$\Omega^{\mathrm{free,reg}} = \frac{N_c}{\pi^2} \sum_{f=u,d} \sum_{s=\pm 1} \int_0^\infty d|\vec{p}|\vec{p}^2(\epsilon + s\mu_f)\Theta(-\epsilon - s\mu_f), \tag{9}$$

where $\epsilon = \sqrt{\vec{p}^2 + m_c^2}$.

The mean field values $\bar{\sigma}$ and $\bar{\pi}$ can now be obtained from a set of two coupled "gap equations" that follow from the minimization of the regularized thermodynamic potential, namely,

$$\frac{\partial\Omega^{\mathrm{MFA,reg}}}{\partial\bar{\sigma}} = 0, \qquad \frac{\partial\Omega^{\mathrm{MFA,reg}}}{\partial\bar{\pi}} = 0. \tag{10}$$

Quark-antiquark and pion condensates are also relevant quantities since they can be taken as order parameters of the spontaneous symmetry breaking transitions. As usual, we consider the scalar condensate $\Sigma = \Sigma_u + \Sigma_d$, where $\Sigma_f = \langle\bar{\psi}_f\psi_f\rangle$; the latter can be obtained by differentiating the thermodynamic potential with respect to the current up and down current quark masses, i.e.,

$$\begin{aligned}\Sigma_f &= \frac{\partial\Omega^{\mathrm{MFA,reg}}}{\partial m_f} \\ &= -2N_c \int \frac{d^4p}{(2\pi)^4}\left[\frac{E_{f'}^2 M(p_f) - \rho(\bar{p})^2(M(p_f) - M(p_{f'}))}{D(\bar{\sigma}, \bar{\pi})} - \frac{m_c}{m_c^2 + p_f^2}\right] \\ &\quad + \frac{N_c m_c}{\pi^2} \sum_{s=\pm 1} \int_0^\infty d|\vec{p}|\vec{p}^2\left(1 + \frac{s\mu_f}{\epsilon}\right)\Theta(-\epsilon - s\mu_f),\end{aligned} \tag{11}$$

where $f' \neq f$. For $\mu_I \neq 0$ one can also have nonvanishing pseudoscalar condensates. According to our choice $\bar{\pi}_i = \delta_{i1}\bar{\pi}$, we define the charged pion condensate $\Pi = \langle \bar{\psi} i\gamma_5 \tau_1 \psi \rangle$. The analytical expression for this quantity can be obtained by taking the derivative of the thermodynamic potential with respect to an auxiliary parameter added to $\rho(\bar{p})$ in Eq. (5), and then set to zero after the calculation [46]. One has

$$\begin{aligned}\Pi &= -4N_c \int \frac{d^4p}{(2\pi)^4} \left\{ \frac{(\rho(\bar{p})+\lambda)[p_u^2 + p_d^2 + 2(\rho(\bar{p})+\lambda)^2 + 2M(p_u)M(p_d) + \mu_I^2]}{(E_u(\lambda)^2 E_d(\lambda)^2 - (\rho(\bar{p})+\lambda)^2)[(M(p_u) - M(p_d))^2 - \mu_I^2]} \right. \\ &\quad \left. - \lambda \frac{p_u^2 + p_d^2 + 2\lambda^2 + 2m_c^2 + \mu_I^2}{(m_c^2 + p_u^2 + \lambda^2)(m_c^2 + p_d^2 + \lambda^2) + \lambda^2 \mu_I^2} \right\} \Big|_{\lambda=0} \\ &= -4N_c \int \frac{d^4p}{(2\pi)^4} \rho(\bar{p}) \frac{E_u^2 + E_d^2 - (M(p_u) - M(p_d))^2 + \mu_I^2}{D(\bar{\sigma}, \bar{\pi})}, \end{aligned} \tag{12}$$

where $E_f(\lambda)^2 = M(p_f)^2 + p_f^2 + (\rho(\bar{p}) + \lambda)^2$.

Finally, as mentioned in the Introduction, it is interesting to study, in this context, the speed of sound, c_s. At zero temperature, one has

$$c_s^2 = \frac{\partial p}{\partial \varepsilon}, \tag{13}$$

where $p = -\Omega^{\mathrm{MFA,reg}}$, while the energy density ε is given by

$$\varepsilon = -p + n_I \mu_I + n_B \mu_B, \tag{14}$$

with $n_I = \partial p / \partial \mu_I$, $n_B = \partial p / \partial \mu_B$. It is also useful to introduce the polytropic index γ [85], given by

$$\gamma = \frac{\partial \ln p}{\partial \ln \varepsilon} = \frac{\varepsilon}{p} c_s^2. \tag{15}$$

In addition, it is interesting to consider the trace anomaly, which is closely related to c_s. Following Ref. [80], we introduce the normalized trace anomaly Δ given by

$$\Delta = \frac{1}{3} - \frac{p}{\epsilon}. \tag{16}$$

In terms of this quantity, the sound velocity squared can be decomposed as

$$c_s^2 = c_{s,\mathrm{deriv}}^2 + c_{s,\mathrm{nonderiv}}^2, \tag{17}$$

where

$$c_{s,\mathrm{deriv}}^2 = -\varepsilon \frac{d\Delta}{d\varepsilon}, \qquad c_{s,\mathrm{nonderiv}}^2 = \frac{1}{3} - \Delta. \tag{18}$$

It should be noted that, from the definition of the polytropic index, these partial contributions can also be expressed as

$$c_{s,\mathrm{deriv}}^2 = \left(1 - \frac{1}{\gamma}\right) c_s^2, \qquad c_{s,\mathrm{nonderiv}}^2 = \frac{1}{\gamma} c_s^2. \tag{19}$$

The trace anomaly tends to vanish if conformal symmetry is approximately restored. Thus, in the conformal limit one has $d\Delta/d\varepsilon \to 0$, $c_s^2 \simeq c_{s,\mathrm{nonderiv}}^2 \to 1/3$, $\gamma \to 1$.

III. NUMERICAL RESULTS

To fully define our model it is necessary to specify the form factor entering the nonlocal fermion current given by Eq. (2). In this work we consider an exponential momentum dependence for the form factor (in momentum space),

$$g(p) = \exp(-p^2/\Lambda^2). \tag{20}$$

This form, which is widely used, guarantees a fast ultraviolet convergence of quark loop integrals. Notice that the energy scale Λ, which acts as an effective momentum cutoff, has to be taken as an additional parameter of the model. Other functional forms, such as, e.g., Lorentzian form factors with integer or fractional momentum dependence, have also been considered in the literature [82,86] (in fact, as stated in the Introduction, the form factor can be fitted to reproduce the momentum dependence of quark propagators obtained from LQCD simulations [40]). In any case, it is seen that the form factor choice, in general, does not have a major impact on the qualitative predictions for most relevant thermodynamic quantities [66].

Given the form factor shape, the model parameters m_c, G, and Λ can be fixed by requiring that the model reproduce the phenomenological values of some selected physical quantities. Here we take as inputs the empirical values of the pion mass, $m_\pi = 138$ MeV, and the pion weak decay constant, $f_\pi = 92.4$ MeV, together with phenomenologically reasonable values of the quark-antiquark condensates at $\mu = \mu_I = 0$, viz. $\Sigma_u = \Sigma_d = -(240\ \mathrm{MeV})^3$. This leads to $m_c = 5.67$ MeV, $\Lambda = 752$ MeV, and $G\Lambda^2 = 20.67$ [81]. In Ref. [46] this parametrization has been used to study the features of this type of model for a system at

finite temperature and isospin chemical potential, getting good agreement with LQCD results for the $T-\mu_I$ phase diagram. As mentioned in the Introduction, one of the aims of this work is to confront the results obtained within the nonlocal model with those obtained in the framework of the standard, local version of the NJL model. For the latter we use the parametrization $m_c = 5.83$ MeV, $\Lambda_0 = 588$ MeV, and $G\Lambda_0^2 = 4.88$, which leads to $\Sigma_u = \Sigma_d = -(239\ \text{MeV})^3$ and quark effective masses $M_u = M_d = 400$ MeV [87].

A. Results for $\mu_B = 0$ and finite μ_I

We begin by stating the picture obtained from the nonlocal NJL model at vanishing baryon chemical potential. It is interesting to compare our results with LQCD calculations, which for $\mu_B = 0$ are free from the sign problem, even for nonzero values of the isospin chemical potential.

1. Order parameters and phase transitions

In Fig. 1 we show the behavior of the above introduced Σ and Π condensates at $\mu_B = 0$ and finite μ_I. Although these results have been previously presented in Ref. [46], we find it convenient to include a brief review for the sake of comparison with the case of nonzero μ_B.

For $\mu_I < m_\pi$ one finds the usual low energy situation in which chiral symmetry is spontaneously broken, which is reflected in a large value $\Sigma = \Sigma_0$ for the quark-antiquark condensate, while the pion condensate vanishes ($\Pi = \Pi_0 = 0$). Then, it can be analytically shown that at $\mu_I = m_\pi$ the model predicts the onset of a phase in which one has pion condensation. For $\mu_I > m_\pi$, as seen in Fig. 1, the chiral condensate decreases monotonically, and the charged pion condensate strongly increases. Thus, one has a second order phase transition in which the isospin symmetry $\mathrm{U}(1)_{I_3}$ gets spontaneously broken, whereas one finds a smooth partial restoration of the $\mathrm{U}(1)_{I_3 A}$ symmetry when reaching large values of μ_I. It can be seen that the results from local and nonlocal versions of the NJL model are similar to each other, and they are found to be in good qualitative agreement with lattice QCD calculations (also shown in the figure) [33]. In addition, as discussed in Ref. [46], for this range of values of μ_I, the results are consistent with the relation

$$\left(\frac{\Sigma}{\Sigma_0}\right)^2 + \left(\frac{\Pi}{\Pi_0}\right)^2 = 1, \tag{21}$$

which can be obtained from lowest-order chiral perturbation theory [88].

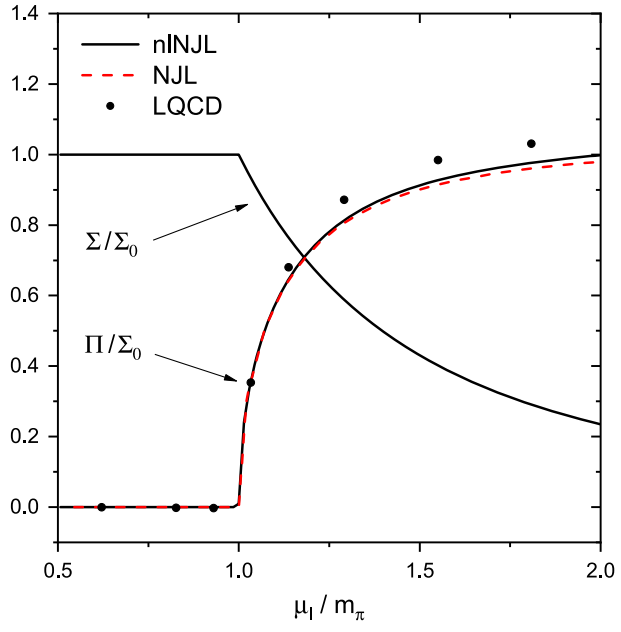

FIG. 1. Normalized Σ and Π condensates as functions of the isospin chemical potential. Lattice results from Ref. [33] are included for comparison.

2. Speed of sound and related quantities

As mentioned above, the speed of sound c_s has been studied within various effective models. For the case of systems at nonzero isospin chemical potential, recent LQCD calculations [24,31] have found that the curve of c_s^2 as a function of μ_I shows a maximum for $\mu_I/m_\pi \sim 2$. This maximum is shown to be well above the conformal limit $c_s^2 = 1/3$. It is worth noticing that a similar behavior has been obtained in the framework of two-color QCD [77,89,90] and quarkyonic models for dense quark matter [91–94].

Our numerical results for the speed of sound c_s^2 and the polytropic index γ are shown in the upper and lower panels of Fig. 2, respectively. For comparison, we also include in both panels the results arising from the local NJL model and those obtained from LQCD in Refs. [24,31]. The calculation of c_s^2 has been carried out by performing the numerical derivative $\partial\varepsilon/\partial\mu_I$ and using $c_s^2 = n_I/(\partial\varepsilon/\partial\mu_I)$, as follows from Eq. (13) for $\mu_B = 0$. To provide an estimate of the dependence on model parametrizations (to be interpreted as a systematic theoretical error of the model), we show gray bands that correspond to the results arising from the nonlocal NJL model for parameters corresponding to quark-antiquark condensates lying within a range from $-(260\ \text{MeV})^3$ to $-(230\ \text{MeV})^3$ (dark gray band), and similarly for the local NJL model, taking in this case a range from $-(250\ \text{MeV})^3$ to $-(240\ \text{MeV})^3$ (light gray band). It can be seen that the results obtained within the nonlocal model do not show a strong dependence on the parametrization. Moreover, they reproduce, with good qualitative agreement, the behavior observed by the most recent LQCD analysis (see Ref. [31]), where a large range of values of μ_I is covered. In the case of the speed of sound, we see that nlNJL results exceed the conformal limit $c_s^2 = 1/3$ at $\mu_I/m_\pi \approx 1.3$,

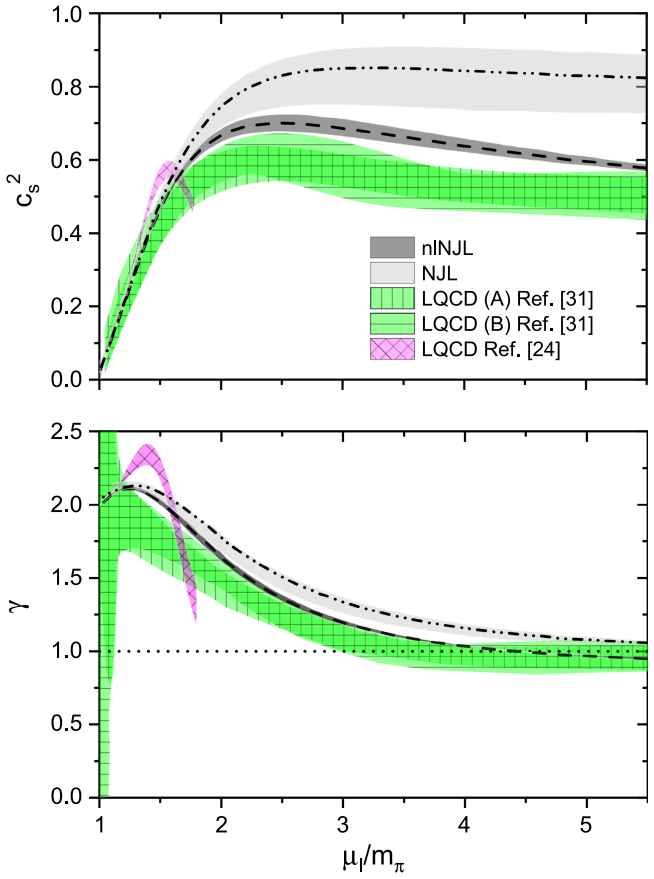

FIG. 2. Squared speed of sound (upper panel) and the polytropic index (lower panel) for $\mu_B = 0$. Dark and light gray bands correspond to the results for local and nonlocal NJL models, respectively, for some ranges of model parameters (see text). The dashed lines within the gray bands correspond to model parametrizations that lead to a quark-antiquark condensate of $-(240\ \mathrm{MeV})^3$. LQCD data from Refs. [24,31] are also included for comparison. The bands correspond, in this case, to statistical errors from lattice simulations.

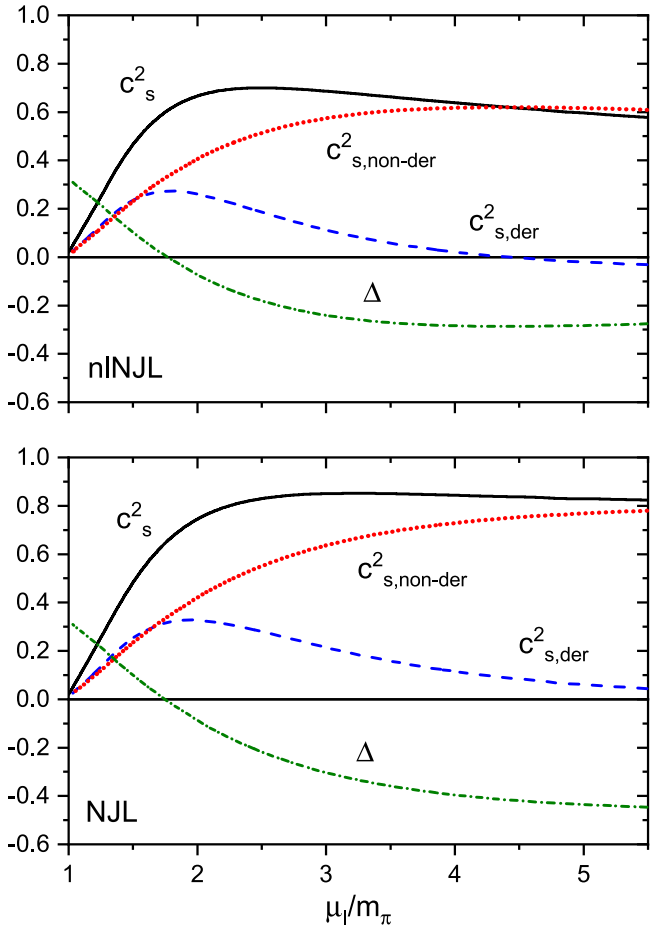

FIG. 3. Contributions to the squared speed of sound for $\mu_B = 0$. Upper and lower panels correspond to nonlocal and local NJL models, respectively, for parametrizations that lead to $\Sigma_f = -(240\ \mathrm{MeV})^3$. The green dashed-dotted lines stand for the normalized trace anomaly Δ.

increasing to a maximum of $c_s^2 \approx 0.7$ at $\mu_I/m_\pi \approx 2.5$ before starting to decrease back towards the conformal value for large values μ_I. On the other hand, in agreement with the results in Ref. [79], it is seen that, for the local NJL model, c_s^2 does not show a clear peak at intermediate values of the isospin chemical potential. In fact, in Ref. [79] it is found that such a peak can be obtained once the coupling constants are allowed to have an explicit dependence on μ_I. In the case of the polytropic index γ, we observe that the results from the nonlocal model are in relatively good agreement with those arising from the LQCD simulation of Ref. [31], which are compatible with values of γ that go below 1 at $\mu_I/m_\pi \gtrsim 4$, before approaching the conformal limit for larger values of μ_I.

The behavior of the normalized trace anomaly Δ and the contributions to c_s^2 defined by Eqs. (16)–(18), for both NJL and nlNJL models, are shown in Fig. 3. Here the results correspond to a quark-antiquark condensate $-(240\ \mathrm{MeV})^3$.

Interestingly, it is seen that for both models the derivative contribution $c^2_{s,\mathrm{deriv}}$ shows a clear peak located close to the point where the conformal relation $\Delta = 0$ is satisfied, i.e., $\mu_I/m_\pi \simeq 1.75$. It should be noticed, however, that the behavior of this quantity for larger values of μ_I is different for both schemes. In the case of the nlNJL model, it decreases rather fast, even becoming slightly negative for the larger values of μ_I considered, a fact that—see Eq. (19)—is consistent with the behavior of the polytropic index γ mentioned above. On the other hand, the decrease is slower in the case of the NJL model, with $c^2_{s,\mathrm{deriv}}$ always remaining positive. The behavior of the nonderivative contribution, although similar for low values of the isospin chemical potential, also differs in the region of large μ_I. We see that while in the case of the nlNJL model this contribution starts to decrease after passing a maximum at $\mu_I/m_\pi \simeq 4$, in the case of the NJL model such a decrease is not observed in the range of μ_I considered. These differences in the behavior of the partial contributions may be attributed

to the extra suppression that appears in the nlNJL model due to the presence of μ_I in the argument of the form factor [see Eq. (6) and the paragraph below]. In turn, they explain why, contrary to the situation in the nlNJL model, for the NJL model the speed of sound does not exhibit a clear peak at intermediate values of μ_I.

B. Phase transitions for finite baryon chemical potential

Let us consider a more general situation in which both the quark chemical potential $\mu = \mu_B/3$ and the isospin chemical potential are nonzero. To describe the picture obtained in the (μ, μ_I) thermodynamic space, we take some representative values of μ and study how the order parameters Σ and Π evolve with μ_I. This is shown in Fig. 4. The left and right panels correspond to the results from nonlocal and local NJL models, respectively.

For low values of μ the situation is similar to the one described in the previous section for $\mu = 0$. In the left and right upper panels of Fig. 4, we show the behavior of Σ and Π for $\mu = 100$ MeV; at $\mu_I/m_\pi = 1$ one finds the onset of a pion condensation phase (a second order phase transition), while chiral symmetry gets smoothly restored when μ_I is increased. Notice that, in the case of the nonlocal model, for large values of μ_I there is a significant deviation from the chiral relation in Eq. (21); this deviation is not observed for the local model (at least for values of μ_I up to $5m_\pi$).

To get a better understanding of the transitions, let us also show contour plots that describe the behavior of the mean field thermodynamic potential $\Omega^{\mathrm{MFA,reg}}$ as a function of the VEVs $\bar{\sigma}$ and $\bar{\pi}$ for particular values of μ_I. In Fig. 5 we consider the case $\mu = 100$ MeV, $\mu_I/m_\pi = 2$. The left and right panels correspond to the nonlocal and local models, respectively. It is seen that, for both models, at $(\bar{\sigma}/\bar{\sigma}_0, \bar{\pi}/\bar{\sigma}_0) \simeq (0.25, 1)$ one finds a solution of the gap equations (10) that minimizes the thermodynamic potential, while a maximum of $\Omega^{\mathrm{MFA,reg}}$ is obtained at $(\bar{\sigma}/\bar{\sigma}_0, \bar{\pi}/\bar{\sigma}_0) = (0, 0)$. The situation is found to be qualitatively similar for larger values of μ_I.

Next, in Fig. 6 we show contour plots for $\mu = 200$ MeV, considering the values $\mu_I/m_\pi = 2$ and $\mu_I/m_\pi = 4(5)$ for the nonlocal (local) model. Comparing the top and bottom panels, it is seen that the maximum located at the axis $\bar{\pi} = 0$ moves to large values of $\bar{\sigma}$, and a second local minimum arises close to the origin. In addition, a saddle point is shown to arise between both local minima. The second minimum represents a metastable point for which there is no pion condensation ($\Pi = 0$); it corresponds to the dashed lines in the central panels of Fig. 4. The onset of this metastable solution occurs at some critical isospin chemical potential that we denote by $\mu_I^{(\mathrm{sp})}$; for the chosen parametrizations, it is seen that $\mu_I^{(\mathrm{sp})}(\mu = 200\ \mathrm{MeV}) \simeq 2m_\pi$ and $4m_\pi$ for the nonlocal and local models, respectively.

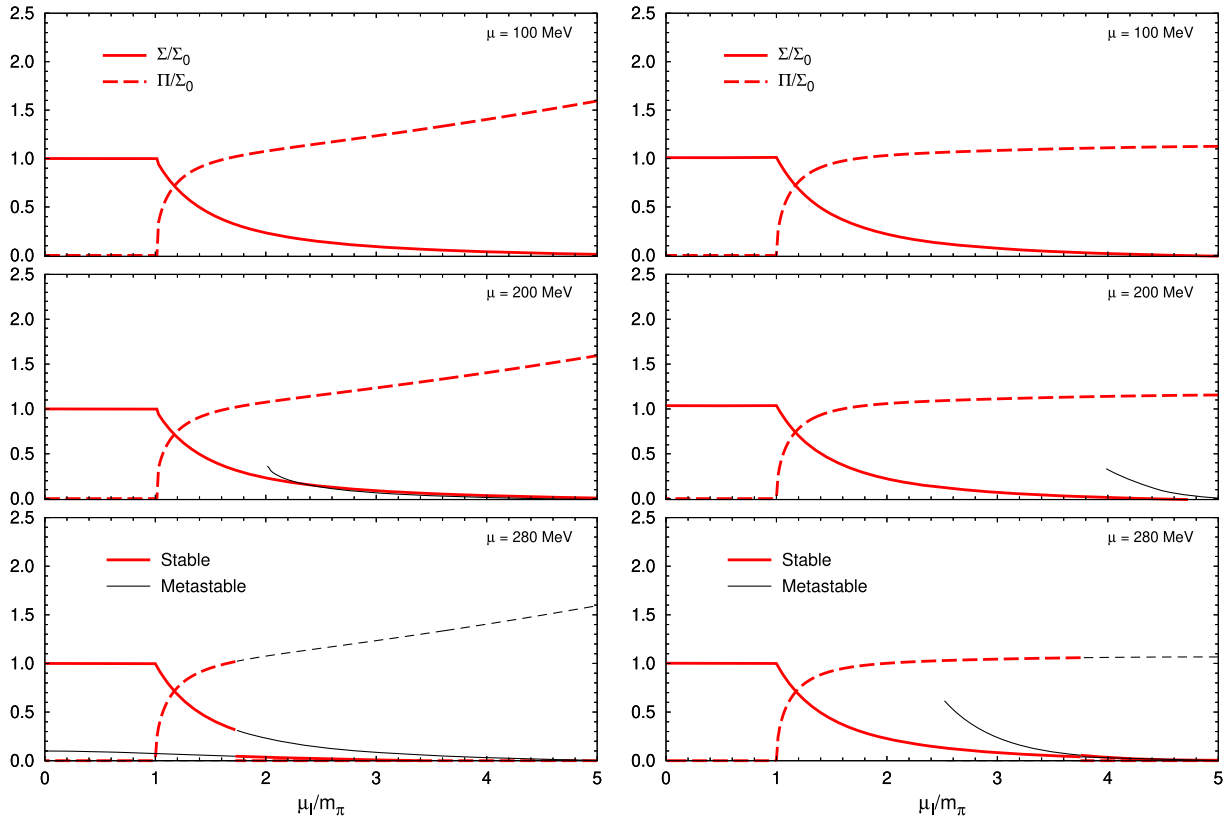

FIG. 4. Normalized values of the order parameters Σ and Π as functions of μ_I/m_π for nonlocal (left) and local (right) NJL models.

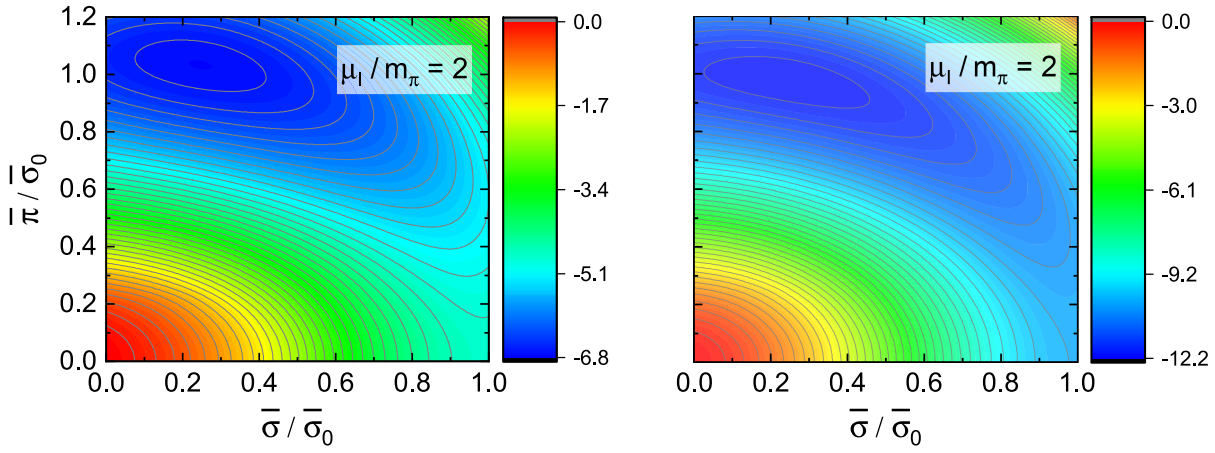

FIG. 5. Contour plots for $\Omega^{\mathrm{MFA,reg}}(\bar{\sigma},\bar{\pi}) \times 10^4$ (in GeV^4) for $\mu = 100$ MeV as functions of $\bar{\sigma}/\bar{\sigma}_0$ and $\bar{\pi}/\bar{\sigma}_0$. The left and right panels correspond to NJL nonlocal and local models, respectively.

We notice that a similar picture has been obtained in Ref. [49] for the case of a three-flavor NJL model. However, in that article the saddle point is interpreted as maximum since only the dependence of the thermodynamical potential with $\bar{\pi}$ is analyzed.

Finally, in Fig. 7 we show how this picture evolves when we go forward to larger values of the chemical potential μ. To illustrate the situation we include some contour plots in which we take $\mu = 280$ MeV and some representative values of μ_I/m_π. As in the previous cases, the left (right)

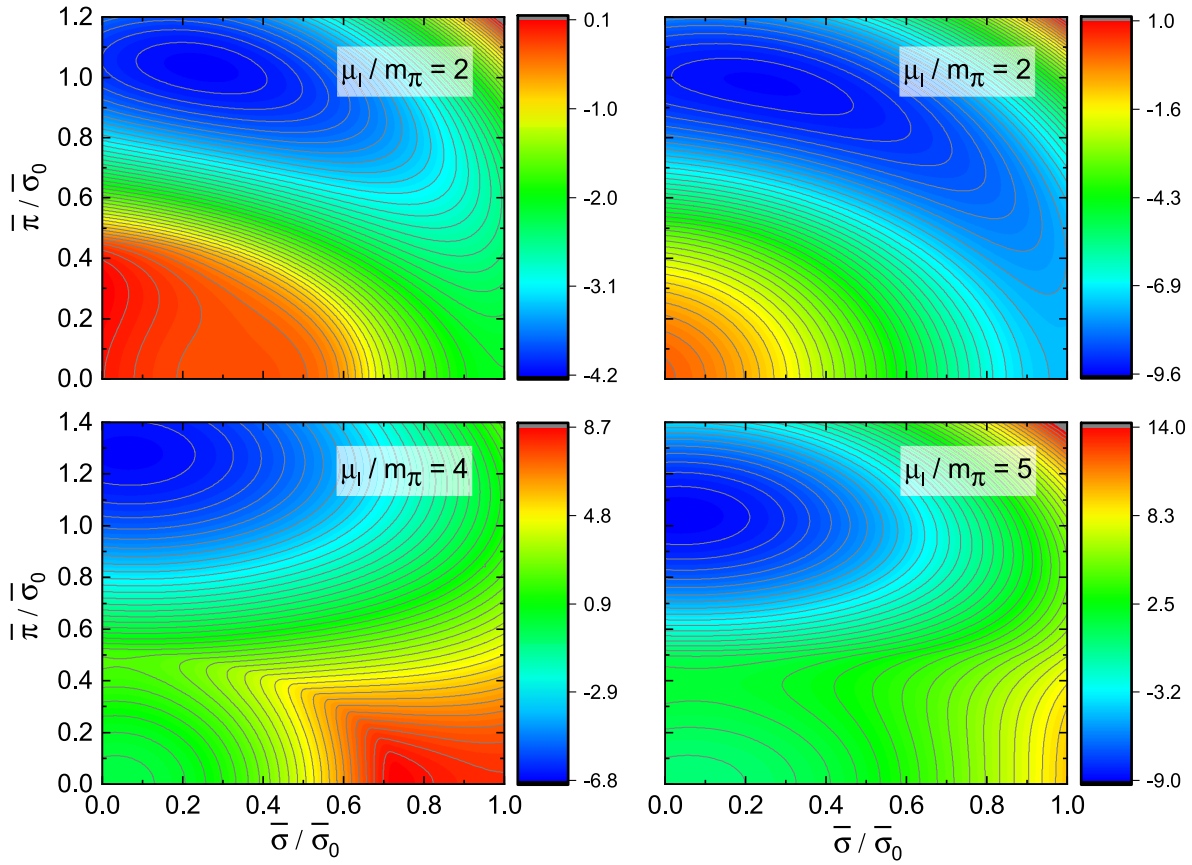

FIG. 6. Contour plots for $\Omega^{\mathrm{MFA,reg}}(\bar{\sigma},\bar{\pi}) \times 10^4$ (in GeV^4) for $\mu = 200$ MeV as functions of $\bar{\sigma}/\bar{\sigma}_0$ and $\bar{\pi}/\bar{\sigma}_0$. The left and right panels correspond to NJL nonlocal and local models, respectively.

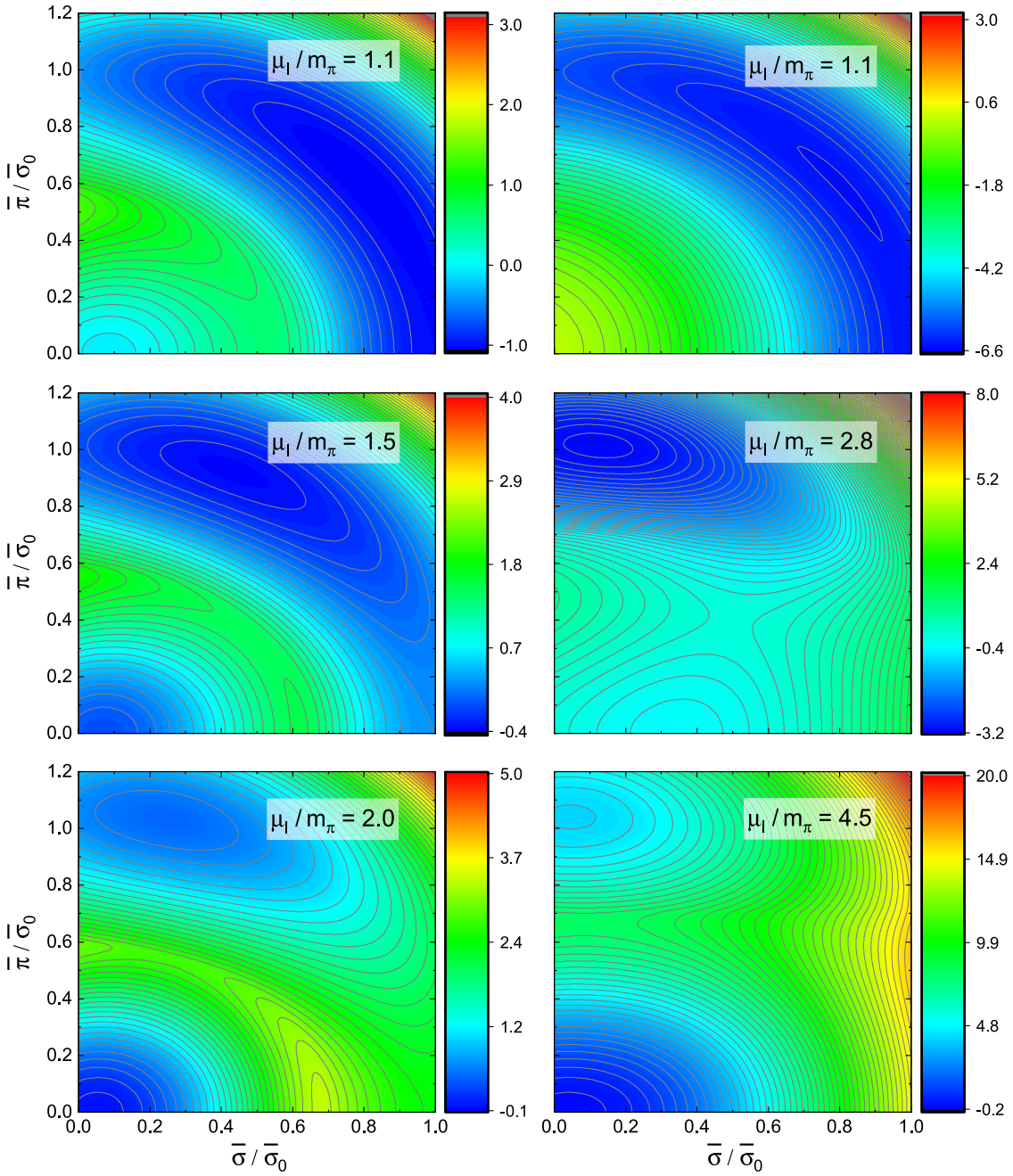

FIG. 7. Contour plots for $\Omega^{\mathrm{MFA,reg}}(\bar{\sigma},\bar{\pi})\times 10^4$ (in GeV^4) for $\mu = 280$ MeV as functions of $\bar{\sigma}/\bar{\sigma}_0$ and $\bar{\pi}/\bar{\sigma}_0$. Left and right panels correspond to NJL nonlocal and local models, respectively.

panels correspond to the nonlocal (local) NJL model. For values or μ_I just above m_π, in the case of the nonlocal model, the metastable solution already exists (in fact, there is no critical value $\mu_I^{(\mathrm{sp})}$ for values of μ larger than about 270 MeV), while for the local model the situation is similar to the one shown in the upper panel of Fig. 6. For larger values of μ_I/m_π (central panels of Fig. 7), in the case of the nonlocal model, the second local minimum becomes deeper, while this second solution also arises for the local model. Then, if μ_I/m_π is further increased, at some critical value $\mu_{I,c}$ a first order phase transition occurs: as illustrated in the lower panels of Fig. 7, the minima for which one has $\bar{\pi} = 0$ are the ones that become energetically favored; thus, the system jumps into a phase in which there is no pion condensation and the $U(1)_{I_3}$ symmetry gets restored. The behavior of the order parameters for $\mu = 280$ MeV is shown in the lower panels of Fig. 4. In the case of the nonlocal model, it is seen that, at the first order transition, the value of the quark-antiquark condensate Σ also shows a jump that implies an approximate restoration of chiral

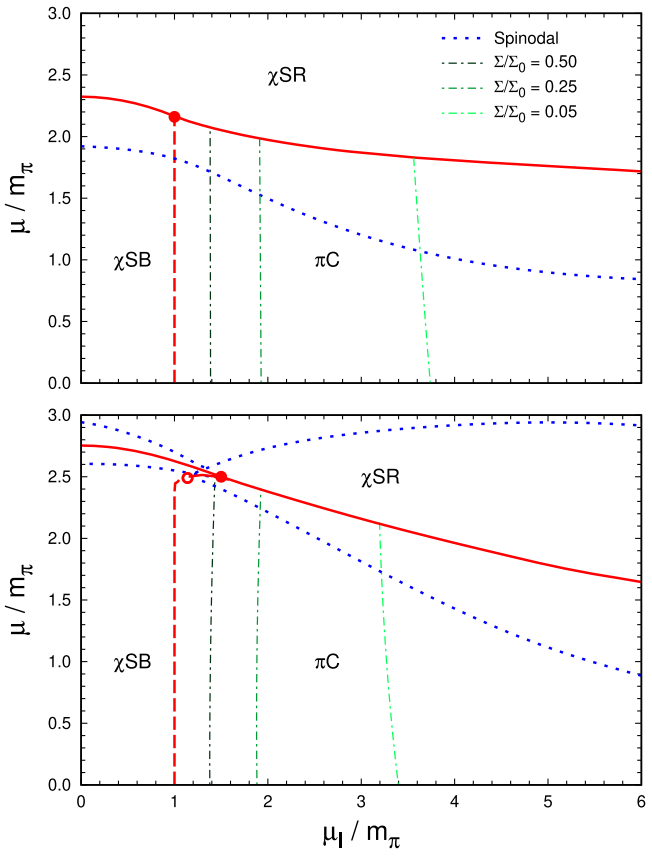

FIG. 8. QCD phase diagram in the $\mu_I - \mu$ plane at zero temperature for the nonlocal (upper panel) and local (lower panel) NJL models. Solid (dashed) lines correspond to first (second) order phase transitions. Here, χSB, πC, and χSR stand for the chiral symmetry broken phase, pion condensation, and the chiral symmetry restored phase, respectively.

symmetry (in the case of the local model, the value of Σ is already very low when the transition is reached).

For even larger values of μ, the region in which there is a stable nonvanishing pion condensate is subsequently reduced, until reaching a triple point in which three phases coexist. The full phase diagrams in the $\mu - \mu_I$ plane for both nonlocal (upper panel) and local (lower panel) models are shown in Fig. 8. Solid and dashed lines denote first and second order phase transitions, respectively, while dotted lines denote the spinodals [84]—boundaries of the region in which energetically unfavored solutions exist as metastable states.

The phase diagrams show a region of normal matter in which one has $\Pi = 0$ and the chiral symmetry is spontaneously broken (χSB), a phase in which $\Pi = 0$ and the chiral symmetry is approximately restored (χSR), and a region in which one finds pion condensation (πC), characterized by a nonvanishing value of Π. In this last region the $U(1)_{I_3 A}$ symmetry is progressively restored when μ_I is increased. As discussed above, for low values of μ the onset of the πC phase is found to occur at $\mu_I = m_\pi$ as a second order phase transition (dashed lines in the figure). The progressive decrease of the chiral order parameter Σ with μ_I [with the consequent partial restoration of the $U(1)_{I_3 A}$ symmetry] is illustrated through the dash-dotted lines, which correspond to constant ratios $\Sigma/\Sigma_0 = 0.5$, 0.25, and 0.05. In this way, for values of μ_I larger enough than m_π, the first order transition indicated by the solid red line occurs between a phase of (almost) massless asymptotically free quarks and a phase of (almost) pure pion condensation.

The filled dots in the figure indicate triple points where two transition lines meet. Notice that in the case of the nonlocal model the second order and first order transition lines meet exactly at $\mu_I = m_\pi$. In contrast, for the local model, the second order transition line has a critical endpoint (open dot in the lower panel of Fig. 8) where it becomes of first order, and then, for $\mu_I > m_\pi$, it smoothly merges with the first order chiral restoration line. Thus, in a narrow region $1.2 \simeq \mu_I/m_\pi \simeq 1.6$ one can find two first order phase transitions when μ is increased: at $\mu \sim 350$ MeV one has a transition from the πC phase to the χSB phase, followed by a transition to the chiral restored phase. In fact, these features of the phase diagram for the local NJL model are in agreement with the results obtained in Refs. [47,49] for two- and three-flavor (local) NJL models.

In Fig. 8 we also show the spinodals, represented by blue dotted lines. As stated, these lines indicate the critical isospin chemical potentials $\mu_I^{(\mathrm{sp})}$ at which metastable solutions are found to appear. For the local NJL model we find spinodals on both sides of the first order transition line—delimiting a band in the phase diagram where metastable solutions exist—while in the case of the nonlocal model no upper spinodal is found. In fact, for large values of μ one can always find a metastable solution in which quarks have a relatively large effective dynamical mass. This is a well-known feature of nonlocal NJL models; it is related to the fact that—depending on the model parametrization—the quark propagators may not have purely real poles in Minkowski space [95].

If one goes further to larger values of μ_I, the nlNJL and NJL approaches show significant differences. For low values of μ, the order parameter Π increases monotonically for the nlNJL model, while for the local model (as shown in Ref. [48]) it starts to decrease and goes to zero at some point beyond $\mu_I \sim 10 m_\pi$. We understand that these different behaviors are artifacts that arise from the regularization of the (nonrenormalizable) models, which become hardly trustable in that limit. Therefore, we present our results for more conservative values of μ_I, up to a few m_π.

The results are not found to show a significant qualitative dependence on the model parametrization for parameter ranges such as those considered in Sec. III A. The main effect on the order parameters falls on Π, whose magnitude can vary within about 15% for $\mu_I \gtrsim 3 m_\pi$. In fact, the effect is similar to the one found at $\mu_B = 0$; see Ref. [46].

The changes have a minor incidence on the phase diagram, which is not found to be significantly modified.

IV. SUMMARY AND CONCLUSIONS

The phase diagram of strongly interacting matter has been examined in two-flavor NJL-type models, considering zero temperature and nonzero baryon and isospin chemical potentials. Specifically, we have investigated the transitions related to the order parameters Σ and Π, which characterize the spontaneous breakdowns of chiral and isospin symmetries, in models with local and nonlocal four-quark interactions. We have also studied the behavior of the speed of sound as a function of the isospin chemical potential.

Considering a $\mu - \mu_I$ phase diagram, for baryon chemical potentials lower than about 280 MeV and $\mu_I < m_\pi$, one finds a region of hadronic matter in which chiral symmetry is spontaneously broken. Then, at $\mu_I = m_\pi$ there is a second order phase transition into a region in which one has a nonzero charged pion condensate. By increasing μ_I the chiral condensate Σ is progressively reduced, implying a smooth restoration of the $\mathrm{U}(1)_{I_3 A}$ symmetry. On the other hand, by increasing μ one arrives at a first order transition to a phase in which there is no pion condensation and the chiral symmetry is approximately restored. In the nonlocal NJL approach it is seen that the first and second order transition lines meet at a triple point located at $\mu_I = m_\pi$, $\mu \simeq 300$ MeV. In the case of the local model, in agreement with previous works, we find that the second order transition line has a critical endpoint where it becomes of first order, and then, for $\mu_I > m_\pi$, it smoothly merges with the first order chiral restoration line. We have also studied metastable phases, identifying saddle points for the thermodynamic potential as a function of the order parameters; in general, it is seen that metastable phases cover a larger region in the case of the nonlocal model. Concerning the speed of sound c_s, we find that for the nonlocal model the behavior of c_s^2 with μ_I for vanishing baryon chemical potential shows a maximum at $\mu_I \sim 2m_\pi$, improving the qualitative agreement with lattice QCD calculations in comparison with the results obtained for the local NJL approach. In the same way, we find some improvement in the predictions for the polytropic index γ.

It would be interesting to extend these studies to systems at finite temperature, with the aim of determining the behavior of the triple point and the phase transition lines (the case $\mu = 0$ has already been considered in Ref. [46]). Typically, one would expect that at some critical temperature the first order transition line between the χSB and χSR phases turns into a smooth crossover. When extending to the finite temperature case one should also consider interactions that involve the Polyakov loop. In the context of the nlNJL model, these interactions have the qualitative effect of producing an increase of the critical transition temperatures [61] and a shift of the critical points towards higher T and lower μ_B in the phase diagram [96]. On the other hand, the limited knowledge of the corresponding Polyakov loop potential would imply a new source of theoretical uncertainty. Finally, it would also be worthwhile to consider the case of neutral matter conditions, to be applied to the composition of compact objects like neutron or pion stars.

ACKNOWLEDGMENTS

This work has been supported in part by Consejo Nacional de Investigaciones Científicas y Técnicas and Agencia Nacional de Promoción Científica y Tecnológica (Argentina), under Grants No. PIP2022-GI-11220210100150CO, No. PICT-2019-00792, and No. PICT20-01847, and by the National University of La Plata (Argentina), Project No. X960.

[1] K. Fukushima and T. Hatsuda, Rep. Prog. Phys. **74**, 014001 (2011).
[2] S. Borsanyi, Z. Fodor, J. N. Guenther, R. Kara, S. D. Katz, P. Parotto, A. Pasztor, C. Ratti, and K. K. Szabo, Phys. Rev. Lett. **125**, 052001 (2020).
[3] M. G. Alford, A. Schmitt, K. Rajagopal, and T. Schäfer, Rev. Mod. Phys. **80**, 1455 (2008).
[4] F. Karsch, Lect. Notes Phys. **583**, 209 (2002).
[5] D. T. Son and M. A. Stephanov, Phys. Rev. Lett. **86**, 592 (2001).
[6] K. Splittorff, D. T. Son, and M. A. Stephanov, Phys. Rev. D **64**, 016003 (2001).
[7] M. Loewe and C. Villavicencio, Phys. Rev. D **67**, 074034 (2003).
[8] D. Toublan and J. B. Kogut, Phys. Lett. B **605**, 129 (2005).
[9] J. O. Andersen, Phys. Rev. D **75**, 065011 (2007).
[10] T. Herpay and P. Kovacs, Phys. Rev. D **78**, 116008 (2008).
[11] K. Kamikado, N. Strodthoff, L. von Smekal, and J. Wambach, Phys. Lett. B **718**, 1044 (2013).
[12] T. Xia, L. He, and P. Zhuang, Phys. Rev. D **88**, 056013 (2013).
[13] H. Ueda, T. Z. Nakano, A. Ohnishi, M. Ruggieri, and K. Sumiyoshi, Phys. Rev. D **88**, 074006 (2013).
[14] R. Stiele, E. S. Fraga, and J. Schaffner-Bielich, Phys. Lett. B **729**, 72 (2014).
[15] T. D. Cohen and S. Sen, Nucl. Phys. **A942**, 39 (2015).
[16] J. O. Andersen, N. Haque, M. G. Mustafa, and M. Strickland, Phys. Rev. D **93**, 054045 (2016).
[17] Z. Zhang and Q. Miao, Phys. Lett. B **753**, 670 (2016).

[18] T. Klahn, T. Fischer, and M. Hempel, Astrophys. J. **836**, 89 (2017).
[19] K. Kashiwa and A. Ohnishi, Phys. Lett. B **772**, 669 (2017).
[20] Z. Wang and P. Zhuang, Phys. Rev. D **96**, 014006 (2017).
[21] B. B. Brandt, G. Endrodi, and S. Schmalzbauer, Phys. Rev. D **97**, 054514 (2018).
[22] K. Aryal, C. Constantinou, R. L. S. Farias, and V. Dexheimer, Phys. Rev. D **102**, 076016 (2020).
[23] P. Adhikari, J. O. Andersen, and M. A. Mojahed, Eur. Phys. J. C **81**, 449 (2021).
[24] B. B. Brandt, F. Cuteri, and G. Endrodi, J. High Energy Phys. 07 (2023) 055.
[25] N. Kovensky, A. Poole, and A. Schmitt, SciPost Phys. **15**, 162 (2023).
[26] M. G. Alford, A. Kapustin, and F. Wilczek, Phys. Rev. D **59**, 054502 (1999).
[27] J. B. Kogut and D. K. Sinclair, Phys. Rev. D **70**, 094501 (2004).
[28] P. de Forcrand, M. A. Stephanov, and U. Wenger, Proc. Sci. LATTICE2007 (**2007**) 237 [arXiv:0711.0023].
[29] P. Cea, L. Cosmai, M. D'Elia, A. Papa, and F. Sanfilippo, Phys. Rev. D **85**, 094512 (2012).
[30] W. Detmold, K. Orginos, and Z. Shi, Phys. Rev. D **86**, 054507 (2012).
[31] R. Abbott, W. Detmold, F. Romero-López, Z. Davoudi, M. Illa, A. Parreño, R. J. Perry, P. E. Shanahan, and M. L. Wagman (NPLQCD Collaboration), Phys. Rev. D **108**, 114506 (2023).
[32] M. Mannarelli, Particles **2**, 411 (2019).
[33] B. B. Brandt, G. Endrodi, E. S. Fraga, M. Hippert, J. Schaffner-Bielich, and S. Schmalzbauer, Phys. Rev. D **98**, 094510 (2018).
[34] G. Ripka, *Quarks Bound by Chiral Fields: The Quark-Structure of the Vacuum and of Light Mesons and Baryons* (Oxford University Press, Oxford, 1997).
[35] Y. Nambu and G. Jona-Lasinio, Phys. Rev. **124**, 246 (1961).
[36] Y. Nambu and G. Jona-Lasinio, Phys. Rev. **122**, 345 (1961).
[37] T. Schäfer and E. V. Shuryak, Rev. Mod. Phys. **70**, 323 (1998).
[38] C. D. Roberts and A. G. Williams, Prog. Part. Nucl. Phys. **33**, 477 (1994).
[39] C. D. Roberts and S. M. Schmidt, Prog. Part. Nucl. Phys. **45**, S1-S103 (2000).
[40] S. Noguera and N. N. Scoccola, Phys. Rev. D **78**, 114002 (2008).
[41] M. B. Parappilly, P. O. Bowman, U. M. Heller, D. B. Leinweber, A. G. Williams, and J. B. Zhang, Phys. Rev. D **73**, 054504 (2006).
[42] S. Furui and H. Nakajima, Phys. Rev. D **73**, 074503 (2006).
[43] K. I. Kondo, Phys. Rev. D **82**, 065024 (2010).
[44] E. Ruiz Arriola and L. L. Salcedo, Phys. Lett. B **450**, 225 (1999).
[45] D. Blaschke, Y. L. Kalinovsky, G. Roepke, S. M. Schmidt, and M. K. Volkov, Phys. Rev. C **53**, 2394 (1996).
[46] J. P. Carlomagno, D. G. Dumm, and N. N. Scoccola, Phys. Rev. D **104**, 074018 (2021).
[47] J. O. Andersen and L. Kyllingstad, J. Phys. G **37**, 015003 (2009).
[48] L. M. Liu, J. Xu, and G. X. Peng, Nucl. Phys. Rev. **40**, 493 (2023).
[49] L. M. Liu, J. Xu, and G. X. Peng, Phys. Rev. D **104**, 076009 (2021).
[50] H. Liu, J. Xu, L. W. Chen, and K. J. Sun, Phys. Rev. D **94**, 065032 (2016).
[51] A. M. Polyakov, Phys. Lett. **72B**, 477 (1978).
[52] K. Fukushima and V. Skokov, Prog. Part. Nucl. Phys. **96**, 154 (2017).
[53] P. N. Meisinger and M. C. Ogilvie, Phys. Lett. B **379**, 163 (1996).
[54] K. Fukushima, Phys. Lett. B **591**, 277 (2004).
[55] E. Megias, E. Ruiz Arriola, and L. L. Salcedo, Phys. Rev. D **74**, 065005 (2006).
[56] C. Ratti, M. A. Thaler, and W. Weise, Phys. Rev. D **73**, 014019 (2006).
[57] S. Roessner, C. Ratti, and W. Weise, Phys. Rev. D **75**, 034007 (2007).
[58] S. Mukherjee, M. G. Mustafa, and R. Ray, Phys. Rev. D **75**, 094015 (2007).
[59] C. Sasaki, B. Friman, and K. Redlich, Phys. Rev. D **75**, 074013 (2007).
[60] D. Blaschke, M. Buballa, A. E. Radzhabov, and M. K. Volkov, Yad. Fiz. **71**, 2012 (2008).
[61] G. A. Contrera, D. Gomez Dumm, and N. N. Scoccola, Phys. Lett. B **661**, 113 (2008).
[62] T. Hell, S. Roessner, M. Cristoforetti, and W. Weise, Phys. Rev. D **79**, 014022 (2009).
[63] T. Hell, S. Rossner, M. Cristoforetti, and W. Weise, Phys. Rev. D **81**, 074034 (2010).
[64] M. Loewe, P. Morales, and C. Villavicencio, Phys. Rev. D **83**, 096005 (2011).
[65] A. E. Radzhabov, D. Blaschke, M. Buballa, and M. K. Volkov, Phys. Rev. D **83**, 116004 (2011).
[66] D. Gomez Dumm, J. P. Carlomagno, and N. N. Scoccola, Symmetry **13**, 121 (2021).
[67] D. Nickel, Phys. Rev. Lett. **103**, 072301 (2009).
[68] D. Nickel, Phys. Rev. D **80**, 074025 (2009).
[69] M. Buballa and S. Carignano, Prog. Part. Nucl. Phys. **81**, 39 (2015).
[70] J. P. Carlomagno, D. Gómez Dumm, and N. N. Scoccola, Phys. Rev. D **92**, 056007 (2015).
[71] L. McLerran and R. D. Pisarski, Nucl. Phys. **A796**, 83 (2007).
[72] H. Abuki, R. Anglani, R. Gatto, G. Nardulli, and M. Ruggieri, Phys. Rev. D **78**, 034034 (2008).
[73] K. Fukushima, Phys. Rev. D **77**, 114028 (2008); **78**, 039902 (E) (2008).
[74] A. Cherman, T. D. Cohen, and A. Nellore, Phys. Rev. D **80**, 066003 (2009).
[75] R. Chiba and T. Kojo, Phys. Rev. D **109**, 076006 (2024).
[76] G. Cao and J. Liao, J. High Energy Phys. 10 (2020) 168.
[77] T. Kojo and D. Suenaga, Phys. Rev. D **105**, 076001 (2022).
[78] C. f. Mu, L. y. He, and Y. x. Liu, Phys. Rev. D **82**, 056006 (2010).
[79] A. Ayala, B. S. Lopes, R. L. S. Farias, and L. C. Parra, arXiv:2310.13130.
[80] Y. Fujimoto, K. Fukushima, L. D. McLerran, and M. Praszalowicz, Phys. Rev. Lett. **129**, 252702 (2022).
[81] D. Gomez Dumm, A. G. Grunfeld, and N. N. Scoccola, Phys. Rev. D **74**, 054026 (2006).

[82] D. Gomez Dumm, S. Noguera, and N. N. Scoccola, Phys. Lett. B **698**, 236 (2011).
[83] D. Ebert, K. G. Klimenko, V. C. Zhukovsky, and A. M. Fedotov, Eur. Phys. J. C **49**, 709 (2007).
[84] D. Gomez Dumm and N. N. Scoccola, Phys. Rev. C **72**, 014909 (2005).
[85] E. Annala, T. Gorda, A. Kurkela, J. Nättilä, and A. Vuorinen, Nat. Phys. **16**, 907 (2020).
[86] J. P. Carlomagno, Phys. Rev. D **97**, 094012 (2018).
[87] M. Buballa, Phys. Rep. **407**, 205 (2005).
[88] J. B. Kogut and D. Toublan, Phys. Rev. D **64**, 034007 (2001).
[89] K. Iida and E. Itou, Prog. Theor. Exp. Phys. (2022) 111B01.
[90] E. Itou and K. Iida, Proc. Sci. LATTICE2022 (**2023**) 151 [arXiv:2210.14385].
[91] L. McLerran and S. Reddy, Phys. Rev. Lett. **122**, 122701 (2019).
[92] K. S. Jeong, L. McLerran, and S. Sen, Phys. Rev. C **101**, 035201 (2020).
[93] N. Kovensky and A. Schmitt, J. High Energy Phys. 09 (2020) 112.
[94] T. Kojo, Phys. Rev. D **104**, 074005 (2021).
[95] D. Gomez Dumm and N. N. Scoccola, Phys. Rev. D **65**, 074021 (2002).
[96] G. A. Contrera, M. Orsaria, and N. N. Scoccola, Phys. Rev. D **82**, 054026 (2010).